

# Longitudinal, 3D Imaging of Collagen Remodeling in Murine Hypertrophic Scars In Vivo Using Polarization-Sensitive Optical Frequency Domain Imaging

William C. Y. Lo<sup>1,2</sup>, Martin Villiger<sup>1</sup>, Alexander Golberg<sup>3,4</sup>, G. Felix Broelsch<sup>5</sup>, Saiqa Khan<sup>5</sup>, Christine G. Lian<sup>6</sup>, William G. Austen Jr<sup>5</sup>, Martin Yarmush<sup>3,7</sup> and Brett E. Bouma<sup>1,2</sup>

Hypertrophic scars (HTS), frequently seen after traumatic injuries and surgery, remain a major clinical challenge because of the limited success of existing therapies. A significant obstacle to understanding HTS etiology is the lack of tools to monitor scar remodeling longitudinally and noninvasively. We present an in vivo, label-free technique using polarization-sensitive optical frequency domain imaging for the 3D, longitudinal assessment of collagen remodeling in murine HTS. In this study, HTS was induced with a mechanical tension device for 4–10 days on incisional wounds and imaged up to 1 month after device removal; an excisional HTS model was also imaged at 6 months after injury to investigate deeper and more mature scars. We showed that local retardation and degree of polarization provide a robust signature for HTS. Compared with normal skin with heterogeneous local retardation and low degree of polarization, HTS was characterized by an initially low local retardation, which increased as collagen fibers remodeled, and a persistently high degree of polarization. This study demonstrates that polarization-sensitive optical frequency domain imaging offers a powerful tool to gain significant biological insights into HTS remodeling by enabling longitudinal assessment of collagen in vivo, which is critical to elucidating HTS etiology and developing more effective HTS therapies.

*Journal of Investigative Dermatology* (2016) 136, 84–92; doi:10.1038/JID.2015.399

## INTRODUCTION

Hypertrophic scars (HTS) are conspicuous, potentially disfiguring lesions that remain a major therapeutic challenge. In fact, its incidence rate after surgery in burn injury is particularly high (>90%) (Gauglitz et al., 2011). Apart from the cosmetic disfigurement, HTS frequently recur and can cause

pruritus, pain, functional impairment, and profound psychological effects.

The pathogenesis of HTS is not fully understood. Its formation typically involves an abnormal wound healing response to trauma, such as burns, inflammation, or surgery, especially when the wound crosses joints or skin creases at right angles (Wolfram et al., 2009). Among other factors, tension is known to be critical to the formation of HTS and, indeed, the well-established surgical treatment—Z-plasty or W-plasty (English and Shenefelt, 1999)—works by relieving tension along the scar. Decreased cellular apoptosis was observed in murine models in which mechanical stress was applied to healing wounds (Aarabi et al., 2007). In addition, overproduction of transforming growth factor- $\beta$  and platelet-derived growth factor suggests the pathologic persistence of wound healing signals (transforming growth factor- $\beta$ 1 and - $\beta$ 2 stimulate collagen synthesis) in HTS (Gauglitz et al., 2011). Histologically, HTS are characterized by the presence of nodular structures with fine, randomly organized collagen bundles (Ehrlich et al., 1994).

To understand scar etiology and assess treatment outcome, imaging is needed. Several imaging techniques have been investigated to assess collagen ex vivo and in vivo. Historically, picrosirius red staining with polarization microscopy, which enhances tissue birefringence (Junqueira et al., 1979), was used to visualize collagen ex vivo. More recently, second-harmonic generation and two-photon excited fluorescence techniques have been used to analyze collagen and

<sup>1</sup>Wellman Center for Photomedicine and Department of Dermatology, Massachusetts General Hospital and Harvard Medical School, Boston, Massachusetts, USA; <sup>2</sup>Harvard-Massachusetts Institute of Technology Division of Health Sciences and Technology, Cambridge, Massachusetts, USA; <sup>3</sup>Center for Engineering in Medicine, Department of Surgery, Massachusetts General Hospital, Harvard Medical School, and the Shriners Burns Hospital, Boston, Massachusetts, USA; <sup>4</sup>Porter School of Environmental Studies, Tel Aviv University, Tel Aviv, Israel; <sup>5</sup>Division of Plastic and Reconstructive Surgery, Massachusetts General Hospital, Harvard Medical School, Boston, Massachusetts, USA; <sup>6</sup>Program in Dermatopathology, Department of Pathology, Brigham & Women's Hospital, Harvard Medical School, Boston, Massachusetts, USA; and <sup>7</sup>Department of Biomedical Engineering, Rutgers University, Piscataway, New Jersey, USA

Correspondence: William C. Y. Lo, Wellman Center for Photomedicine and Department of Dermatology, Massachusetts General Hospital and Harvard Medical School, 50 Blossom Street, Boston, Massachusetts 02114, USA. E-mail: Lo.William@mgh.harvard.edu

Abbreviations: DOP, degree of polarization; HTS, hypertrophic scars; LR, local retardation; OCT, optical coherence tomography; PS, polarization-sensitive; PS-OFDI, polarization-sensitive optical frequency domain imaging

Received 24 January 2015; revised 28 September 2015; accepted 29 September 2015; accepted manuscript published online 8 October 2015

elastin, respectively, in ex vivo HTS and keloid specimens (Chen et al., 2009; Vogler et al., 2011). Unfortunately, these techniques only offer a limited field of view and are challenging to use in vivo. Optical coherence tomography (OCT) offers fast imaging speed, increased field of view, and imaging depth, at a spatial resolution suitable for biological applications, which makes it particularly amenable to in vivo imaging. OCT has been investigated for the imaging of skin (Alex et al., 2010; Gambichler et al., 2011), and in particular for the imaging of burn scars (Gong et al., 2013) and skin cancer (Mogensen et al., 2009).

Polarization-sensitive OCT is an extension of OCT that also measures the polarization state of the light backscattered by the sample. It enables the measurement of tissue birefringence, primarily caused by fibrillar collagen, in the skin. Polarization-sensitive OCT has been shown to provide intrinsic contrast in thermally damaged tissue, thereby providing a tool for burn depth assessment (De Boer et al., 1998; Park et al., 2001; Pierce et al., 2004a, 2004b) and mapping of dermal birefringence in photoaged skin (Sakai et al., 2008) in vivo.

In this study, we present the use of polarization-sensitive optical frequency domain imaging (PS-OFDI), a variant of polarization-sensitive OCT that offers improved imaging speed and sensitivity (Villiger et al., 2013), for the 3D imaging of a rat model of surgical HTS in vivo. This animal model employs a mechanical tension device placed on healing incisional wounds, which enables the systematic study of HTS formation (Aarabi et al., 2007). To validate PS-OFDI in imaging deeper scars, we also investigated an excisional wound scar placed under autologous tension, imaged at 6 months after injury. We evaluate both local retardation (LR) and degree of polarization (DOP), computed using our spectral binning algorithm (Villiger et al., 2013), for enhancing the contrast of HTS, which, to the best of our knowledge, has not been reported previously. Compared with cumulative retardation, LR expresses the rate of change of the measured polarization states with depth, and is a direct, more intuitive measure of tissue birefringence. DOP is a quantity related to the randomness of the detected polarization states of light, which scales from zero for completely random to unity for perfectly uniform polarization states. Unlike LR, DOP captures the cumulative effect of the tissue from the surface to a given depth. We observed that the combination of LR and DOP provides a robust optical signature to differentiate HTS given the presence of fine, densely packed collagen bundles in HTS compared with thicker collagen bundles in normal skin.

In addition, we demonstrate the use of PS-OFDI for studying HTS remodeling by imaging the incisional wound model longitudinally for 1 month and the excisional model at 6 months. Interestingly, we observed a progressive increase in LR and a persistently high DOP within the scar region over time, which corresponded well with the remodeling and thickening of collagen fibers histologically. Normalization of the scar was associated with an increased LR and decreased DOP back to baseline levels in normal skin. Our findings suggest that PS-OFDI can serve as a valuable 3D imaging tool for the noninvasive, longitudinal assessment of HTS in vivo, by providing significant biological insights into collagen

remodeling central to understanding HTS etiology and monitoring therapeutic response to improve current therapies and investigate novel approaches.

## RESULTS

### Imaging aberrant collagen organization in HTS using PS-OFDI

Figure 1 shows the cross-sectional PS-OFDI images of a mechanical tension-induced HTS after 10 days of loading (imaged 1 month later) compared with normal rat skin. For intuitive visualization, the LR and DOP signals were merged with the intensity image (as a brightness channel) and displayed using an isoluminant colormap (Geissbuehler and Lasser, 2013). Whereas conventional intensity images show minimal contrast (only slightly increased backscattering), the local retardation (PS-LR) and degree of polarization (PS-DOP) images demonstrate significant differences in HTS compared with normal skin. HTS shows significantly reduced LR and increased DOP deep inside the dermis, compared with heterogeneous LR and low DOP beyond the epidermis in normal skin. This optical signature (reduced LR and high DOP) corresponds histologically to thin, less organized collagen bundles in HTS (Figure 1d), compared with thicker collagen bundles in normal skin (Figure 1h). These abnormal collagen bundles are cigar-shaped and orientated parallel to the surface of the skin along the tension lines of the scar tissue (Figure 1d). In addition, there is an increased cellularity of fibroblasts in HTS compared with normal skin (Figure 1d and h).

### Histological correlation

We further analyzed the histological correlation of the PS-OFDI images in each animal group with varying duration of tension (Figure 2). In all cases, the scar region shows reduced LR and increased DOP. Overall, the PS-DOP images correlate well with the extent and shape of the scar as confirmed by hematoxylin and eosin histology (Figure 2c, f, i, and l), whereas the PS-LR images show more variability. The size of HTS also increased with the duration of tension, as expected, from a barely noticeable scar with minimal deposition of collagen in the 4-day group (Figure 2c) to a significantly larger scar extending all the way through the dermis that is characterized by aberrant collagen bundles and increased cellularity of dermal fibroblasts in the 10-day group (Figure 2l).

### Longitudinal, 3D imaging of HTS in vivo

A major advantage of using PS-OFDI, compared with conventional histology processing, is the ability to assess HTS longitudinally and comprehensively in vivo (Figure 3), which is particularly important for studying HTS etiology and assessing response. By imaging the incisional HTS model (6-day group) at 1-week intervals after device removal, we observed rapid contraction of the scar in the first week, as indicated by the normalization of DOP and LR around the boundary of the scar to baseline levels in normal skin (increased LR and decreased DOP). From weeks 1 to 4, the scar continued to remodel progressively, leading to a further reduction in scar size and an interesting increase in LR, particularly in deeper regions. The DOP remained persistently high within the scar region. To investigate the evolution of the LR and DOP signals further, we analyzed the PS-LR and

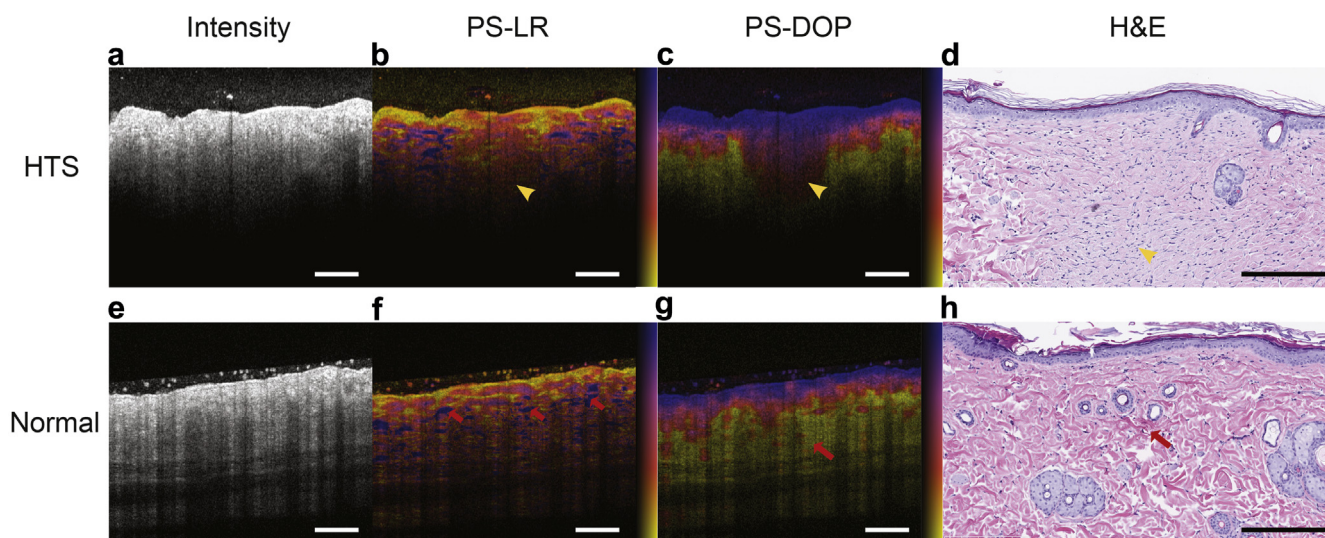


**Figure 1. Visualization of tension-induced HTS and normal skin in vivo using PS-OFDI (10-day group).** Intensity (a, e), local retardation (LR) (b, f), degree of polarization (DOP) (c, g) images and the corresponding hematoxylin and eosin (H&E) histology (d, h) are shown for HTS (a–d) and normal skin (e–h). HTS exhibits reduced LR (approximately  $0.3 \text{ deg}/\mu\text{m}$  in the region indicated by yellow arrowheads) and high DOP (1.0) corresponding to thin, densely packed collagen fibers (d), whereas normal skin contains islands of high LR (approximately  $0.8 \text{ deg}/\mu\text{m}$  in regions indicated by red arrows) and generally low DOP (approximately  $0.3\text{--}0.5$ ) in the dermis corresponding to thick, mature, more loosely distributed collagen (h). Color bars range from 0 to  $1.2 \text{ deg}/\mu\text{m}$  for PS-LR and 0.5 to 1 for PS-DOP images, respectively. HTS, hypertrophic scars; PS-OFDI, polarization-sensitive optical frequency domain imaging. Scale bars =  $500 \mu\text{m}$  (a–c, e–g),  $250 \mu\text{m}$  (d, h).

PS-DOP images at three major time points (Figure 4). After the initial incision (and before the application of tension), the fresh incisional wound (at day 2) was marked by a small region with very low LR and high DOP (Figure 4a and b), which expanded significantly after loading the healing incision for 8 days (Figure 4c and d). As the tension-induced wound continued to remodel over the 1-month period, LR increased significantly whereas DOP remained high (Figure 4e and f). Finally, we analyzed the relative maturity of the collagen using Herovici's method (Herovici, 1963), which has been shown and used to distinguish young, newly formed collagen (blue) from more mature, highly cross-linked collagen (purple/red) in previous studies (Krötzsch-Gómez et al., 1998; Lillie et al., 1980; Ozog et al., 2013; Turner et al., 2013). As shown by Herovici's staining and Ki67/SMA staining, the change in LR over the 1-month period corresponded well with the transition from a scar with thin, newly formed (blue) collagen and myofibroblasts at week 0 to thicker, more mature (purple) collagen bundles with decreased cellularity at week 4 (Figure 5).

#### Imaging a mature excisional HTS model in vivo

To demonstrate the clinical utility of our approach in imaging deeper full-thickness scars, we performed our imaging experiments in an excisional wound 6 months after the injury. Interestingly, we observed a much more prominent increase in LR deep in the dermis at 6 months (Figure 6a), which corresponds well with more organized, thicker collagen fibers deep in the dermis with decreased cellularity (Figure 6e), compared with thinner and less organized collagen fibers surrounded by a high density of fibroblasts in the HTS region closer to the epidermis with a lower LR (Figure 6d). In both cases, the DOP within the scar remained significantly higher than in normal skin (Figure 6b).

#### DISCUSSION

This study demonstrated the use of PS-OFDI for 3D, label-free imaging of murine models of HTS, thereby enabling noninvasive, quantitative evaluation of scar remodeling longitudinally. Interestingly, we observed that the remodeling of collagen is correlated with a significant increase in LR in both the incisional and excisional HTS models. This ability to probe HTS in vivo allows us to gain significant biological insights into collagen remodeling, which plays a central role in wound healing. Whereas the excisional wound model provides a convenient approach to study deeper scars that are more difficult to treat clinically, the incisional wound model with a tension device provides an elegant way to control the size of the scar systematically (e.g., by varying the duration of tension placement) as shown here.

Unlike previous studies employing polarization-sensitive OCT for the characterization of skin and scar tissue (De Boer et al., 1998; Park et al., 2001; Pierce et al., 2004a, 2004b; Sakai et al., 2008), we reconstructed the LR (instead of cumulative retardation), which reflects tissue birefringence more closely and is much more intuitive to interpret. LR expresses how much the birefringence of the tissue rotates the polarization states at each depth, whereas cumulative retardation compares the polarization states at a given depth with respect to the surface (resulting in increasing values even in uniform tissue with constant birefringence). In addition, we computed DOP, which provides a useful metric to identify and measure HTS. Our expression of DOP is similar to the degree of polarization uniformity established by Göttinger et al. (2008); however, here we employ a spectral binning algorithm and spatial averaging to reduce noise (Villiger, 2013). DOP captures the uniformity of the measured polarization states in a small region of interest. In a homogeneous tissue, the polarization states of neighboring pixels are

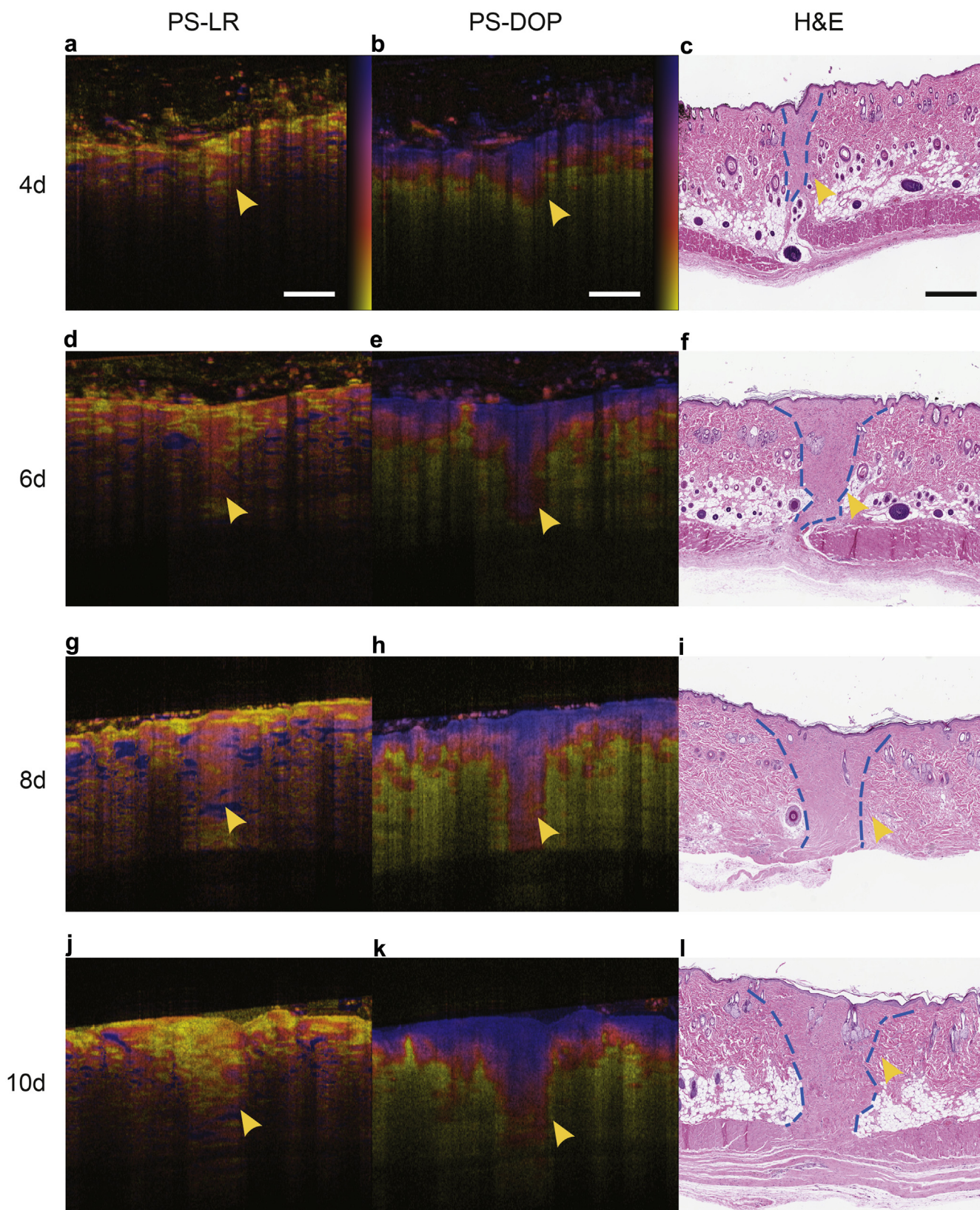


**Figure 2. Histological correlation of PS-OFDI images in 4-day (a–c), 6-day (d–f), 8-day (g–i), and 10-day (j–l) groups.** (a, d, g, j) PS-LR images, (b, e, h, k) PS-DOP images, and (c, f, i, l) hematoxylin and eosin (H&E) histology. Each animal was tattooed with a set of ink marks around the scar for coregistration. Yellow arrowheads, scar region. Dotted blue lines, scar area on H&E. Color bars range from 0 to 1.2 deg/ $\mu\text{m}$  for PS-LR and 0.5 to 1 for PS-DOP images, respectively. PS-DOP, polarization-sensitive degree of polarization; PS-LR, polarization-sensitive local retardation; PS-OFDI, polarization-sensitive optical frequency domain imaging. Scale bars = 500  $\mu\text{m}$ .

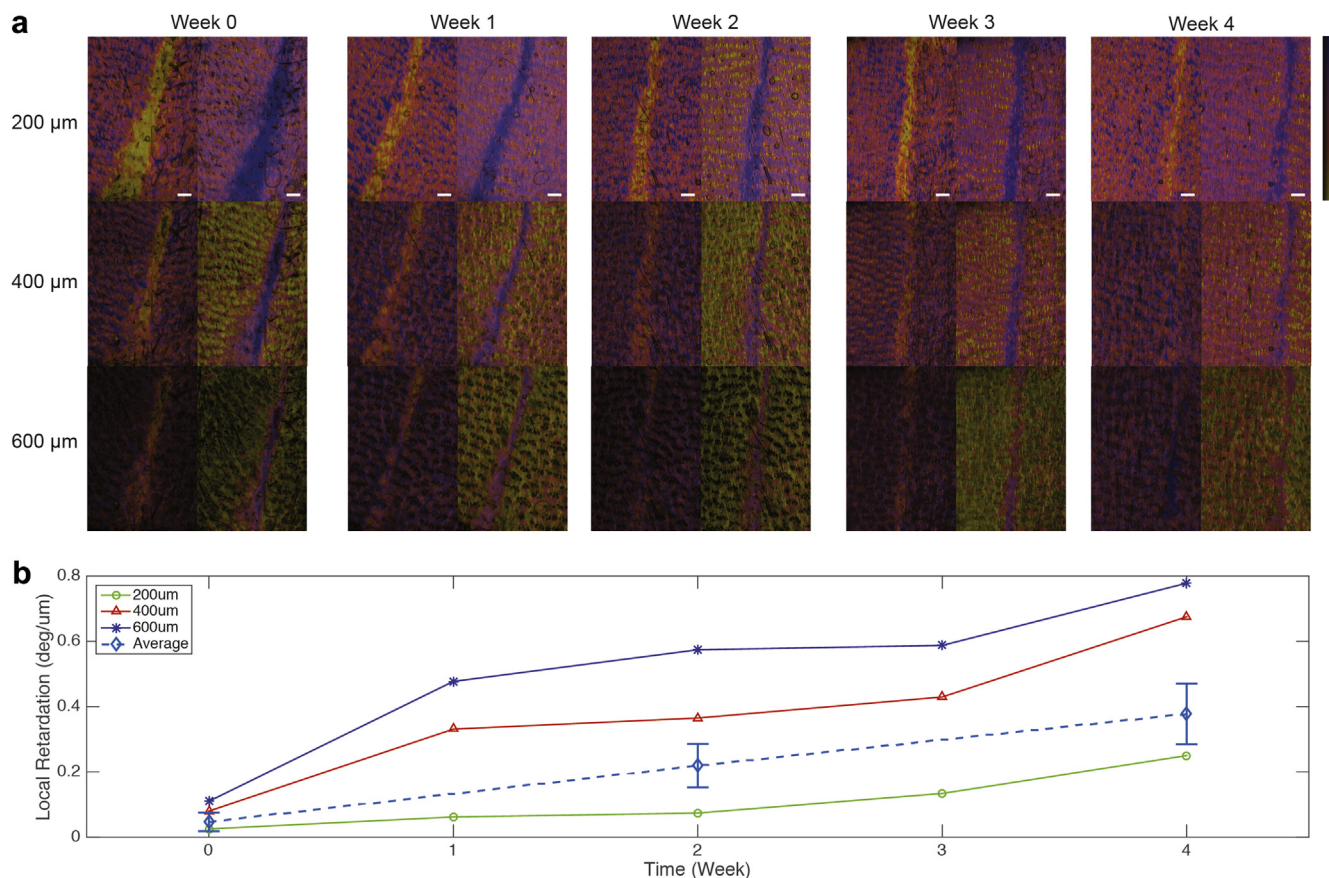


**Figure 3. Longitudinal imaging of the tension-induced HTS model for 1 month after tension device removal, showing rapid scar remodeling from weeks 0 to 1, followed by a more progressive phase from weeks 1 to 4. (a)** Left column: PS-LR images, right column: PS-DOP images at each time point. Images represent *enface* average intensity projection across a 100-μm section at indicated depths. Color bars range from 0 to 1.2 deg/μm for PS-LR and 0.5 to 1 for PS-DOP images, respectively. Scale bars = 500 μm. **(b)** As the collagen fibers remodeled, LR increased progressively at each depth, particularly in deeper regions, whereas DOP remained high. The average local retardation ( $n = 3$  animals), computed in cross-sectional slices covering the entire scar, showed a similar trend. Values represent the mean  $\pm$  SD. HTS, hypertrophic scars; PS-DOP, polarization-sensitive degree of polarization; PS-LR, polarization-sensitive local retardation.

expected to be very similar. In heterogeneous tissues, where two adjacent image pixels potentially interrogate two differently oriented collagen bundles, they are more likely to differ and reduce the measured DOP.

Using LR and DOP, we were able to clearly differentiate normal skin from HTS because of the very different collagen architecture in each case. In normal skin, the heterogeneous, mesh-like organization of highly organized collagen bundles give rise to islands of high dermal birefringence in PS-LR images, alternating with areas of low birefringence due to the varying alignment of the bundles with respect to the optical imaging axis. Furthermore, the spatial dimensions of the region of interest required for the generation of the PS-LR and PS-DOP images frequently include several bundles, accentuating the heterogeneous appearance of normal skin. This heterogeneity also explains the rapid decrease of DOP beyond the epidermis. In contrast, HTS are characterized by finer and microscopically less organized collagen that exhibits lower dermal birefringence, increasing over time as the fibers remodel and thicken. HTS are optically more homogeneous and preserve the polarization state of the incident light, resulting in high DOP values deep within the dermis. In addition, the epidermis and papillary dermis typically

showed reduced LR values and also preserved the polarization state of the incident light, leading to a high DOP.

In our validation study, the HTS area measured with PS-OFDI showed the expected dependence with the duration of tension and matched well with histological assessment of the same region. DOP provides a measure of the HTS area in the dermis and LR tends to be more variable particularly as the collagen fibers mature. In contrast, DOP typically remains high throughout scar remodeling. One limitation of DOP is that superficial layers normally exhibit high DOP values, which can make it difficult to assess the lateral extent of the scar on the surface.

Our histological analysis confirmed that there is significant HTS formation after placing the device for 8–10 days. Although the area of scar formation was increased in the 4-day and 6-day groups compared with the control group, histological features of HTS were not as evident. This is consistent with an earlier report suggesting that the duration of tension was critical to HTS formation and that at least 7 days of continuous loading was required in a mouse model (Aarabi et al., 2007). It is fascinating that our rat model showed not only significantly increased the scar area in the 10-day group, but also similar histopathological features of

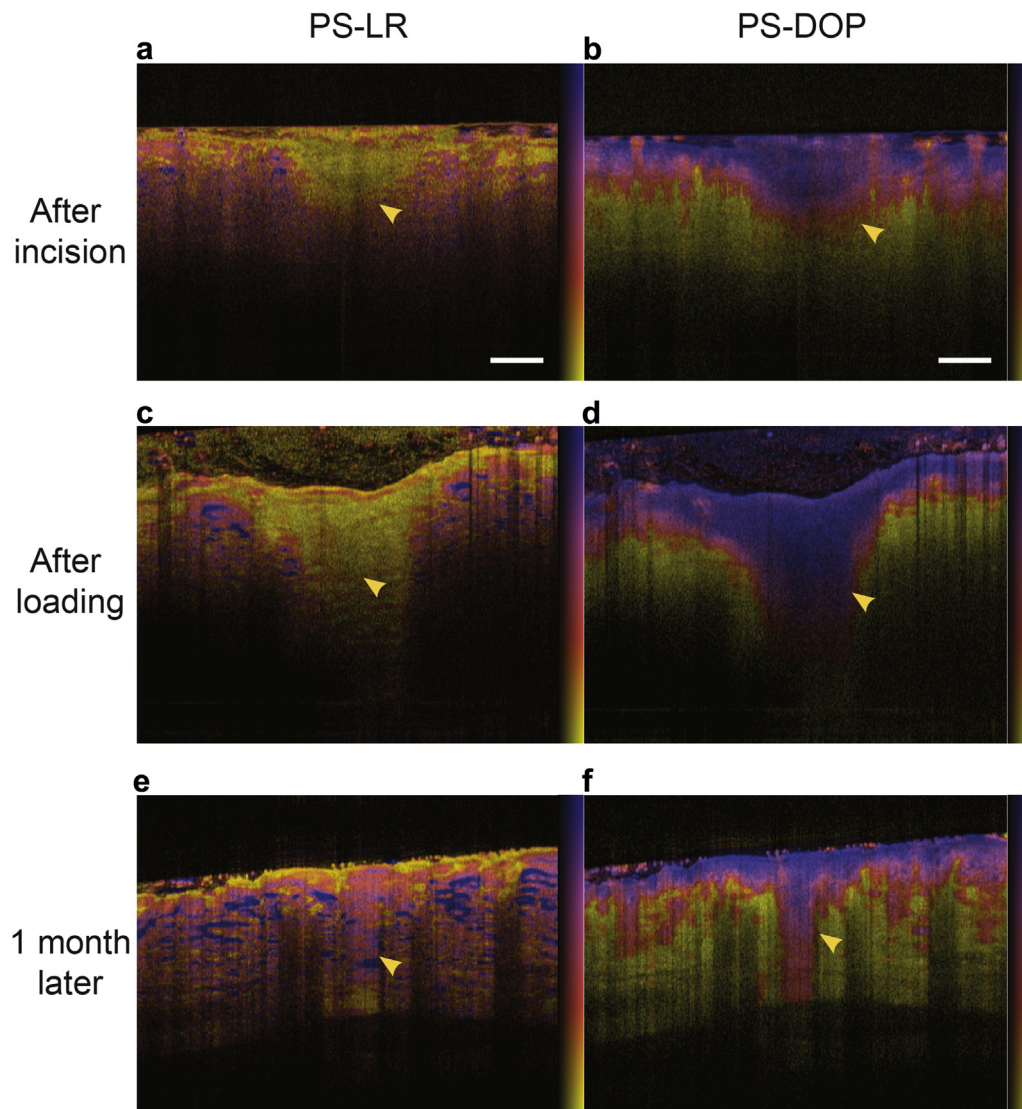


**Figure 4. Cross-sectional PS-LR and PS-DOP images at major time points providing insights into collagen remodeling during wound healing: before tension loading (a, b), after tension loading (c, d), and 1 month after tension device removal (e, f).** Tension loading led to the rapid expansion of the scar compared with the initial unloaded incisional wound, as revealed by the region (yellow arrowheads) with extremely low LR and high DOP (after incision: LR = 0.03 deg/ $\mu$ m, DOP = 1.0; after loading: LR = 0.08 deg/ $\mu$ m, DOP = 1.0). As the tension-loaded incisional wound healed over the 1-month period, the scar region was marked by increased LR (approximately 0.4 deg/ $\mu$ m) and high DOP (0.98). Color bars range from 0 to 1.2 deg/ $\mu$ m for PS-LR and 0.5 to 1 for PS-DOP images, respectively. PS-DOP, polarization-sensitive degree of polarization; PS-LR, polarization-sensitive local retardation. Scale bars = 500  $\mu$ m.

HTS in human tissue including increased cellularity of fibroblasts and a dermal nodule with haphazard orientation of collagen bundles.

Finally, this study demonstrated 3D, longitudinal assessment of an HTS model in vivo at high resolution. We observed rapid remodeling of the scar in the first week after tension device removal, followed by a more progressive remodeling phase, including the emergence of a region with increased birefringence but high DOP deep within the scar. Interestingly, the increase in LR corresponded well with the transition from a highly cellular, immature scar with thin collagen fibers at week 0 to a less cellular, more mature scar with thicker collagen fibers at week 4. Our excisional HTS study at 6 months further suggests that LR can be used as a surrogate for collagen remodeling, whereas DOP can be used to monitor the size of HTS during the remodeling process.

Currently, there is a lack of high-resolution imaging tools to study wound healing and scar formation systematically and longitudinally in vivo. Given that collagen plays a critical role in the pathogenesis of abnormal wound healing, it is an important target for imaging. Increased collagen synthesis by fibroblasts with the expression of transforming growth factor- $\beta$  and platelet-derived growth factor, and decreased collagen degradation with reduced MMP activity are hallmarks of this process (Wolfram et al., 2009). In fact, a study demonstrated the use of transforming growth factor- $\beta$ 1 and - $\beta$ 2 neutralizing antibodies in rats to prevent scar formation in dermal wounds (Shah et al., 1992). Therefore, our label-free, high-resolution imaging technique can serve as a promising tool to gain significant insights into wound healing by monitoring both scar size (using DOP) and collagen remodeling (using LR) longitudinally. For example, healing of the scar increases the

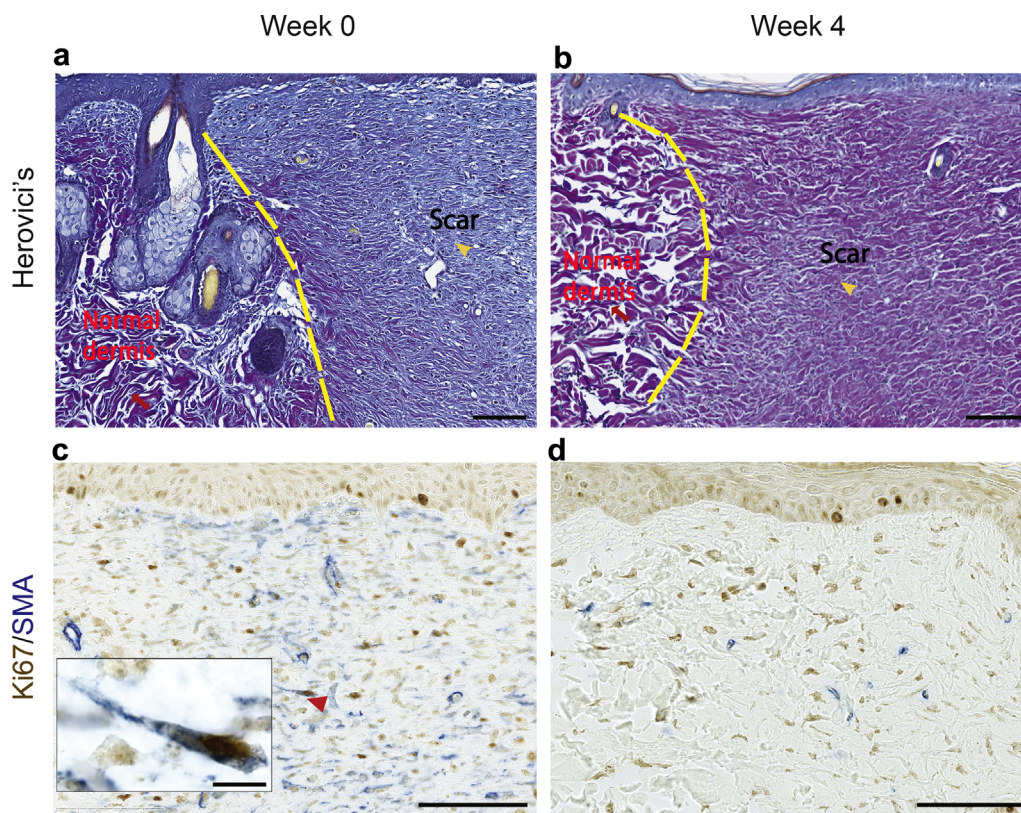


**Figure 5. Histology of HTS immediately after tension loading (a, c) and 1 month after device removal (b, d), showing significant collagen remodeling within the scar tissue.** At week 0, immediately after tension loading, the incisional wound contained an abundance of thin, newly formed collagen (blue), compared with surrounding normal skin with thicker, more mature collagen (purple), as indicated by Herovici's staining (a), as well as proliferating myofibroblasts (Ki67/SMA+, see inset) (c), indicating a phase of an acute tissue reaction. At week 4, the scar region transitioned to more mature, thicker collagen (b), and a significantly lower density of fibroblasts (with decreased SMA and Ki67 positivity) (d). A representative section is shown at each time point. Scale bars = 100  $\mu$ m (10  $\mu$ m in inset). Yellow arrowheads, scar region; red arrows, normal dermis (a, b). Red arrowhead, Ki67/SMA+ myofibroblast shown in inset (c). Ki67, brown; SMA, blue (c, d). HTS, hypertrophic scars.

LR signal and decreases the DOP back to values observed in normal skin.

Indeed, most of our current therapeutic approaches for treating HTS rely on targeting or reversing the abnormal collagen deposited during wound healing. For example, intralesional injection of corticosteroids is thought to decrease fibroblast proliferation and collagen synthesis, whereas pulsed dye laser treatment is thought to favor collagen degradation and fibroblast apoptosis (Kuo et al., 2005; Urioste et al., 1999). However, the lack of noninvasive scar imaging techniques in well-established animal models for HTS has hindered the study of HTS formation in vivo, especially at earlier time points because most studies relied on surgical scar specimens harvested months after their formation. Therefore, the ability to assess collagen in vivo in an animal model of HTS, as demonstrated in this paper, enables further investigation to explore novel, targeted therapeutic approaches for HTS, which is the subject of our ongoing studies. In addition, the PS-OFDI technique can be directly applied to imaging human HTS in vivo as we expect a similar optical signature (decreased LR and increased DOP) given the similarity in collagen organization, namely the presence of fine collagen fibers with haphazard orientation in a dermal nodule. Clinically, this noninvasive, high-resolution 3D scar imaging capability can be exploited to improve the management of HTS, including the initial

assessment and longitudinal monitoring of treatment response in patients.

## MATERIALS AND METHODS

### Animals

Six-week-old female Sprague-Dawley rats (approximately 200 g, N = 18) were purchased from Charles River Laboratories (Wilmington, MA). The animals were housed in individual cages with access to food and water ad libitum, and were maintained on a 12-hour light-dark cycle in a temperature-controlled room. All animal procedures were approved by the Subcommittee on Research Animal Care (IACUC) of the Massachusetts General Hospital (protocol number 2012N000077) and were in accordance with the guidelines of the National Institutes of Health (NIH).

**Tension-induced surgical HTS model in rats.** A biomechanical loading device was constructed from 22-mm expansion screws and metal supports, which allows the device to be placed over a healing incision without contacting the wound. The procedure was developed based on a previous report by Aarabi et al. (2007). After the induction of anesthesia with isoflurane, two 2-cm linear full-thickness incisions were made on the dorsum (5 cm apart—one at the cranial end and another at the caudal end) and then reapproximated with three 4-0 vicryl sutures. On postincision day 4, the sutures were removed from the healing incisions, and the loading

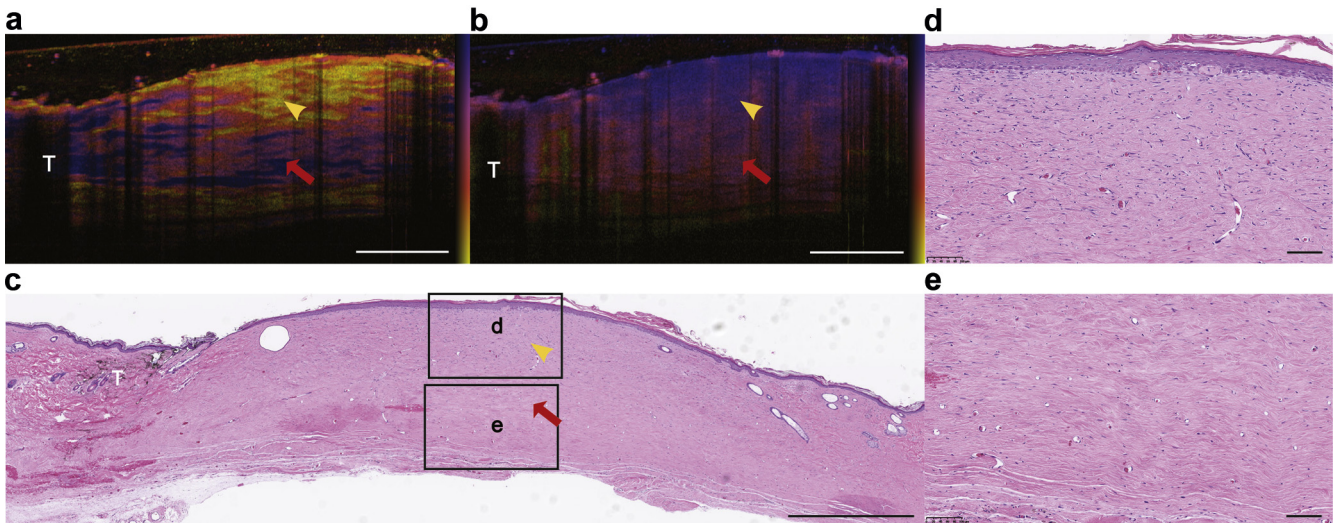


**Figure 6.** Excisional HTS model imaged 6 months after injury with PS-OFDI, demonstrating the ability to probe collagen remodeling noninvasively over long periods of time in deeper scars. The top region with low LR (0.2 deg/μm) (yellow arrowhead) in the PS-LR image (a) and high DOP (1.00) in the PS-DOP image (b) corresponds histologically to the scar region with an abundance of fibroblasts and relatively thin, disorganized collagen bundles (d), whereas the region with higher LR (0.9 deg/μm) (red arrow) and high DOP (0.96) corresponds to thicker, more organized collagen bundles in the dermis and relatively few fibroblasts (e). T, tattoo mark. Color bars range from 0 to 1.2 deg/μm for PS-LR and 0.5 to 1 for PS-DOP images, respectively. HTS, hypertrophic scars; PS-DOP, polarization-sensitive degree of polarization; PS-LR, polarization-sensitive local retardation; PS-OFDI, polarization-sensitive optical frequency domain imaging. Scale bars = 1 mm (a–c), 100 μm (d, e).

device was carefully secured with 6-0 nylon sutures on one of the incisions. The second incision served as a control.

Tension on the wound was created by translating the expansion screws by 2 mm at the time of securing the loading device, and 2 mm every day thereafter. This was necessary to prevent stress relaxation because of the natural elongation of the skin resulting in a decrease in the tension on wounds. At the end of the loading period (4, 6, 8, or 10 days), the device was removed and the scar was imaged 1 month later (or at 1-week intervals for the longitudinal study). Histological analysis was performed at week 0 and week 4 (see [Supplementary Methods](#) online for details).

**Excisional HTS model in rat.** A 2.5 cm × 2 cm full-thickness excisional wound was created on the mid dorsum. The lax skin flanking the wound was gathered with a running 4-0 vicryl suture to create tension. On each side of the wound, excess skin was gathered in a running fashion starting at the cephalic aspect, down to the caudal aspect, and back up to the cephalic end. The length of the gathered skin was the length of the wound created (2.5 cm). The small ridge of skin produced was tacked down laterally. This was performed on each side of the wound to secure the tension. A small piece of gauze and Tegaderm were placed over the wound. The sutures were left until reabsorbed (approximately 2 weeks after excision). Buprenorphine (0.05 mg/kg) was administered subcutaneously every 12 hours up to 72 hours after excision.

#### PS-OFDI system

The PS-OFDI system used in this study has been reported in detail previously ([Villiger et al., 2013](#)). A wavelength-swept laser source operating at a center wavelength of 1,320 nm with an axial resolution of 9.4 μm was used. The A-line rate was 54 kHz and the signal was digitized at 85 MHz. In the reference arm, an acousto-optic modulator was used to remove depth degeneracy ([Yun et al., 2004](#)). An imaging window of 10 × 5 mm, consisting of 2,048 A-lines/image × 256 images, was scanned with a focused beam featuring a lateral resolution of 15 μm. The skin was apposed against

a glass slide with ultrasound gel as immersion liquid to center the superficial layers in focus. The polarization state of the input light was modulated between circular and linear polarization between adjacent A-lines, and the signal was detected with a polarization diverse receiver.

Reconstruction of the PS data was performed with spectral binning ([Villiger et al., 2013](#)), using one-fifth of the original spectral bandwidth (i.e., nine overlapping spectral bins), a lateral Gaussian filter of a full width at half maximum equal to 12 adjacent A-lines, and an axial offset of 48 μm to derive the LR. The DOP was evaluated independently for each spectral bin and input polarization state over the same lateral Gaussian kernel, and then averaged:

$$DOP = \frac{1}{2N} \sum_{p=1}^2 \sum_{n=1}^N \frac{\sqrt{Q_{p,n}^2 + U_{p,n}^2 + V_{p,n}^2}}{I_{p,n}},$$

where  $Q$ ,  $U$ ,  $V$ , and  $I$  are the spatially averaged, but unnormalized components of the Stokes vector,  $p$  denotes the input polarization states, and  $n$  denotes the spectral bin.

#### CONFLICT OF INTEREST

The authors state no conflict of interest.

#### ACKNOWLEDGMENTS

Research reported in this publication was funded in part by the National Institutes of Health P41 EB015903 grant and by the Shriners Foundation grant no. 85120-BOS. WCYL was supported by the Canadian Institutes of Health Research (CIHR) Doctoral Foreign Study Award and MV was supported by the Swiss National Science Foundation.

#### SUPPLEMENTARY MATERIAL

Supplementary material is linked to the online version of the article at [www.jidonline.org](http://www.jidonline.org), and at [doi:10.1038/JID.2015.399](https://doi.org/10.1038/JID.2015.399).

#### REFERENCES

Aarabi S, Bhatt KA, Shi Y, et al. Mechanical load initiates hypertrophic scar formation through decreased cellular apoptosis. *FASEB J* 2007;21:3250–61.

- Alex A, Považay B, Hofer B, et al. Multispectral in vivo three-dimensional optical coherence tomography of human skin. *J Biomed Opt* 2010;15:026025-1–15.
- De Boer J, Srinivas S, Malekafzali A, et al. Imaging thermally damaged tissue by polarization sensitive optical coherence tomography. *Opt Express* 1998;3:212–8.
- Chen G, Chen J, Zhuo S, et al. Nonlinear spectral imaging of human hypertrophic scar based on two-photon excited fluorescence and second-harmonic generation. *Br J Dermatol* 2009;161:48–55.
- Ehrlich HP, Desmoulière A, Diegelmann RF, et al. Morphological and immunochemical differences between keloid and hypertrophic scar. *Am J Pathol* 1994;145:105–13.
- English RS, Shenefelt PD. Keloids and Hypertrophic Scars. *Dermatol Surg* 1999;25:631–8.
- Gambichler T, Jaedicke V, Terras S. Optical coherence tomography in dermatology: technical and clinical aspects. *Arch Dermatol Res* 2011;303:457–73.
- Gauglitz GG, Korting HC, Pavicic T, et al. Hypertrophic scarring and keloids: pathomechanisms and current and emerging treatment strategies. *Mol Med* 2011;17:113–25.
- Geissbuehler M, Lasser T. How to display data by color schemes compatible with red-green color perception deficiencies. *Opt Express* 2013;21:9862–74.
- Gong P, McLaughlin RA, Liew YM, et al. Assessment of human burn scars with optical coherence tomography by imaging the attenuation coefficient of tissue after vascular masking. *J Biomed Opt* 2013;19:021111-1–10.
- Götzinger E, Pircher M, Geitzenauer W, et al. Retinal pigment epithelium segmentation by polarization sensitive optical coherence tomography. *Opt Express* 2008;16:16410–22.
- Herovici C. A polychrome stain for differentiating precollagen from collagen. *Stain Technology* 1963;38:204–5.
- Junqueira LCU, Bignolas G, Brentani RR. Picrosirius staining plus polarization microscopy, a specific method for collagen detection in tissue sections. *Histochem J* 1979;11:447–55.
- Kröttsch-Gómez FE, Furuzawa-Carballeda J, Reyes-Márquez R, et al. Cytokine expression is downregulated by collagen-polyvinylpyrrolidone in hypertrophic scars. *J Invest Dermatol* 1998;111:828–34.
- Kuo Y-R, Wu W-S, Jeng S-F, et al. Activation of ERK and p38 kinase mediated keloid fibroblast apoptosis after flashlamp pulsed-dye laser treatment. *Lasers Surg Med* 2005;36:31–7.
- Lillie RD, Tracy DRE, Pizzolato P, et al. Differential staining of collagen types in paraffin sections: a color change in degraded forms. *Virchows Arch A Path Anat and Histol* 1980;386:153–9.
- Mogensen M, Thrane L, Jørgensen TM, et al. OCT imaging of skin cancer and other dermatological diseases. *J Biophotonics* 2009;2:442–51.
- Ozog DM, Liu A, Chaffins ML, et al. Evaluation of clinical results, histological architecture, and collagen expression following treatment of mature burn scars with a fractional carbon dioxide laser. *JAMA Dermatol* 2013;149:50–7.
- Park BH, Saxer C, Srinivas SM, et al. In vivo burn depth determination by high-speed fiber-based polarization sensitive optical coherence tomography. *J Biomed Opt* 2001;6:474–9.
- Pierce MC, Sheridan RL, Hyle Park B, et al. Collagen denaturation can be quantified in burned human skin using polarization-sensitive optical coherence tomography. *Burns* 2004a;30:511–7.
- Pierce MC, Strasswimmer J, Hyle Park B, et al. Birefringence measurements in human skin using polarization-sensitive optical coherence tomography. *J Biomed Opt* 2004b;9:287–91.
- Sakai S, Yamanari M, Miyazawa A, et al. In vivo three-dimensional birefringence analysis shows collagen differences between young and old photodamaged human skin. *J Invest Dermatol* 2008;128:1641–7.
- Shah M, Foreman DM, Ferguson MWJ. Control of scarring in adult wounds by neutralising antibody to transforming growth factor  $\beta$ . *Lancet* 1992;339:213–4.
- Turner NJ, Pezzone MA, Brown BN, et al. Quantitative multispectral imaging of Herovici's polychrome for the assessment of collagen content and tissue remodelling. *J Tissue Eng Regen Med* 2013;7:139–48.
- Urioste SS, Arndt KA, Dover JS. Keloids and hypertrophic scars: review and treatment strategies. *Semin Cutan Med Surg* 1999;18:159–71.
- Villiger M, Zhang EZ, Nadkarni SK, et al. Spectral binning for mitigation of polarization mode dispersion artifacts in catheter-based optical frequency domain imaging. *Opt Express* 2013;21:16353–69.
- Vogler N, Medyukhina A, Latka I, et al. Towards multimodal nonlinear optical tomography — experimental methodology. *Laser Phys Lett* 2011;8:617–24.
- Wolfram D, Tzankov A, Püzl P, et al. Hypertrophic scars and keloids—a review of their pathophysiology, risk factors, and therapeutic management. *Dermatol Surg* 2009;35:171–81.
- Yun S, Tearney G, de Boer J, et al. Removing the depth-degeneracy in optical frequency domain imaging with frequency shifting. *Opt Express* 2004;12:4822–8.